Electrochimica Acta xxx (xxxx) 143586

Contents lists available at ScienceDirect

Electrochimica Acta

journal homepage: www.elsevier.com/locate/electacta

Effective photoelectrocatalysis of levofloxacin antibiotic with $Ti/IrO_2—Nb_2O_5$ in environmental samples

Carlos H.M. Fernandes [a, *], Lorena A. Goulart [b], Roger Gonçalves [b], Géssica O.S. Santos [a], Maria V.B. Zanoni [c], Lucia H. Mascaro [b], Marcos R.V. Lanza [a, *]

[a] Institute of Chemistry of São Carlos, University of São Paulo, 13566-590 SP Brazil
[b] Department of Chemistry, Federal University of São Carlos, 13560-970 SP Brazil
[c] Institute of Chemistry, São Paulo State University (UNESP), 14800-060 SP Brazil

ARTICLE INFO

Keywords:
Real water
Iridium-Niobium-based electrode
Photoelectrocatalysis
Antibiotics
Pechini method
Advanced oxidation process

ABSTRACT

This work reports the development and application of a highly efficient catalyst based on IrO_2 and Nb_2O_5 for the degradation of the antibiotic Levofloxacin (LFX) in simulated and real surface water samples. The $IrO_2—Nb_2O_5$ films, which were obtained by modified Pechini method, were deposited on a titanium substrate, leading to the production of $Ti/IrO_2—Nb_2O_5$ electrode. After being subjected to morphological, structural and electrochemical characterization, the $Ti/IrO_2—Nb_2O_5$ electrode was applied for the degradation of LFX using different processes, including electrolysis (EC) and photoelectrolysis (PhEC), and the results obtained were compared to that of UV–Vis irradiation-based photolysis. The application of the PhEC process led to a relatively higher and faster removal of LFX in the water matrices investigated, where 100% degradation rate and about 70% mineralization rate were obtained at the end of 1.5 h of treatment, compared to the individual photolysis and EC processes. The results obtained from quenching tests showed that LFX degradation under the PhEC process may be associated with the presence of active radicals, such as $HO^{\bullet}$, $SO_4^{\bullet-}$ and $O_2^{\bullet-}$, in addition to the e^-/h^+ pair formed with the incidence of light during treatment. Apart from excellent photoelectrocatalytic activity and high stability, the $Ti/IrO_2—Nb_2O_5$ electrode exhibited high electrochemically active surface area (ECSA). The excellent results obtained from the application of the PhEC process in terms of TOC removal and the remarkable catalytic properties of $Ti/IrO_2—Nb_2O_5$ point to the high efficiency of the system proposed in this study when applied for the treatment and removal of organic pollutants from real water samples.

1. Introduction

The prevalence and detection of pharmaceutical contaminants (PCs), such as antibiotics, in aquatic systems is an issue of huge concern worldwide [1]. These substances can reach aquatic environment mainly by wastewater treatment plants (WWTPs), (which are not primary designed to treat such recalcitrant species that came from industries, hospital and households) and due to direct use of veterinary medicine and in aquaculture leading to a great release of PCs in the environment [2,3]. A large quantity of these recalcitrant compounds is usually found in an unmetabolized form [4]. Continuous exposure of drugs to the aqueous environment, even at low concentration levels, has been found to pose substantial and long-term risks to humans and animals [5]. Seasonal variations also tend to affect the prevalence and concentration levels of the pharmaceutical contaminants found in aqueous matrices; the highest concentrations of these compounds are often detected during the winter because of the increased consumption of medicine during this period, as people are more prone to various diseases [6–7].

The antibiotic levofloxacin (LFX) is considered an emerging pollutant due to its low degradability in WWTPs, which makes it highly prevalent in the aqueous environment [3]. Due to its wide spectrum of activity and efficiency bacteria, LFX has been commonly applied for the treatment of pneumonia, bacterial rhinosinusitis, bacterial exacerbation of chronic bronchitis, bacterial prostatitis, pyelonephritis, urinary tract infection, infectious diseases of the skin or skin structures, among other diseases [8–9]. Owing to the widespread consumption of LFX and its high toxicity, as well as its persistence in the environment coupled with its possible endocrine disrupting effects, it is essentially important to develop highly efficient methods that are capable of effectively re-

* Corresponding authors.
E-mail addresses: chmfernandes@usp.br (C.H.M. Fernandes), marcoslanza@usp.br (M.R.V. Lanza).

https://doi.org/10.1016/j.electacta.2023.143586
Received 8 July 2023; Received in revised form 16 November 2023; Accepted 26 November 2023

moving this compound (and their toxicity) from real aqueous matrices or converting to low toxicity and biodegradable by-products [2,10].

Over the past few decades, powerful advanced oxidation processes (AOPs) and electrochemical advanced oxidation processes (EAOPs) have been developed and applied for the removal of organic pollutants from contaminated water and wastewater [11–12]. The use of this kind of processes for the treatment of organic pollutants has sparked considerable interest among researchers because their application leads to the formation of highly oxidizing radicals, including hydroxyl (•OH, E^0 = 2.7 V vs normal hydrogen electrode [NHE]) and sulfate radicals (SO_4•−, E^0 = 3.1 V vs. NHE) [13]. Recently, sulfate radical-based AOPs (SR-AOP) has been received great attention due to its high capability of reaction with several organic compounds at nearly diffusion controlled rates (comparable to •OH). In addition, since SO_4•− reacts with organics through single-electron transfer, this leads to SO_4•− present a higher selectivity to react with contaminant containing aromatic π electrons, electron-rich groups, or unsaturated bonds, besides SO_4•− longer lifetime (30–40 μs) compared to •OH (20 ns) enables more stable mass transfer and contact with contaminants allowing a more efficient degradation.

Among the wide range of EAOPs reported in the literature, photoelectrocatalysis (PhEC) has been found to produce excellent results when applied for the removal of organic compounds; these outstanding results are attributed to the direct and/or indirect degradation mechanisms that occur in the treatment process and which involve the formation of charges and oxidants with the incidence of light [14]. As pointed out in the literature, the main limitation of the PhEC process lies in the material employed as photocatalyst. There has been an increasingly growing interest among researchers regarding the use of photoanodes with high stability, good electrical conductivity, and high photocatalytic activity as photocatalysts in the PhEC process as a way of circumventing this underlying constraint and boosting the efficiency of the process.

Mixed metal oxides, including iridium oxide (IrO_2) and ruthenium oxide (RuO_2), have become widely employed as catalytic materials in electrochemical oxidation processes due to their high oxidation capacity and good conductivity [15–16]. It should be noted however that due to their high price, RuO_2 and IrO_2 have often been applied in combination with other cheaper metal oxides in order to reduce the material costs [17–20]. Niobium and tantalum oxides are usually employed in combination with catalytic oxides to increase the mechanical stability of the electrodes [21–22]. Considering that Brazil is one of the largest producers of niobium ore, this makes the production of Nb-based materials highly viable in the country [15,23]. Niobium pentoxide (Nb_2O_5) is a transition metal oxide and an *n*-type semiconductor with a band gap of about 3.4 eV; this oxide has attracted considerable attention among researchers due to its high catalytic performance and good stability in aqueous media [24–26]. When applied in small quantities in combination with other semiconductor oxides, Nb_2O_5 can dramatically increase the photocatalytic activity of these materials [27–28]. Unlike other semiconductor oxides, such as TiO_2, ZnO, and WO_3, which have been long explored as photocatalytic materials, the highly promising Nb_2O_5 photocatalytic material has only been recently explored as a photocatalyst despite possessing good catalytic properties.

Taking the above considerations into account, the present study sought to investigate the photoelectrocatalytic activity of electrodes based on IrO_2 and Nb_2O_5 and their application for the degradation of LFX in different water matrices. Specifically, we employed advanced oxidation (AO) technologies for the treatment of real water, as the application of these AO processes helps demonstrate the great potential and efficiency of the treatment technique proposed in this study. The results obtained from this study show that the combined application of IrO_2 and Nb_2O_5 leads to the formation of electrodes with high stability and excellent photocatalytic activity which promote the effective degradation of recalcitrant pollutants in real samples.

2. Experimental

2.1. Chemicals

All the chemicals, including citric acid (CA - a.r. Synth), ethylene glycol (EG - a.r., Synth), $K_2IrCl_6.xH_2O$ (a.r. Sigma-Aldrich), $NH_4NbO(C_2O_4)_2$ (a.r., Sigma-Aldrich), oxalic acid (a.r., Synth), HCl (a.r., JT Baker), H_2SO_4 (Merck), Na_2SO_4 (Merck) and Levofloxacin (Sigma-Aldrich), employed in the experiments were used as received and without further purification. All solutions were prepared using deionized water (Millipore Milli-Q system with a resistivity of 18.2 MΩ cm).

2.2. Synthesis of the proposed electrodes

The $Ti/IrO_2—Nb_2O_5$ electrodes were prepared by the modified Pechini method, as described in our previous study [15]. Initially, Ti plates (99.7%, 1 cm × 1 cm) were treated by sandblasting, followed by chemical etching in boiling solutions of HCl (1:1 *w/w*) and then in oxalic acid (10% *w/w*) for 30 min. The substrates were then rinsed with deionized water and dried with N_2 gas flow. In the meantime, a resin containing CA, EG, and metal salts was prepared by initially dissolving citric acid in ethylene glycol at 60 °C. To this mixture, a certain amount of the metal salt ($K_2IrCl_6.xH_2O$ and $NH_4NbO(C_2O_4)_2$) was added in order to obtain a final molar ratio of 1(Ir(0.40)/Nb(0.60)):4(CA):16(EG) and produce the nominal composition of the desired $IrO_2—Nb_2O_5$ films. After the complete dissolution of the metal salts, the resulting solution was brush-painted on the Ti substrate. After that, the electrodes were initially treated at 130 °C for 30 min and later at 250 °C for 10 min. Finally, the electrodes were treated again at 500 °C for 10 min to eliminate all organic polymers and promote the formation of the desired oxides. These procedures (i.e., from brush-painting to the heat treatments) were repeated 10 times before further characterization or application of the $Ti/IrO_2—Nb_2O_5$ electrodes for the degradation of levofloxacin.

2.3. Electrode characterization

Morphological and structural characterizations of the $Ti/IrO_2—Nb_2O_5$ electrodes were carried out using the following analytical methods: *i*) scanning electron microscopy with field emission gun (FEG-SEM Zeiss model Supra 35VP) equipped with a high-resolution secondary electron detector (in-lens detector), operating at 6.0 kV with a point-to-point resolution of 3.8 nm; and *ii*) X-ray diffraction (XRD) using RU200B Rigaku Rotaflex, under a step scan mode in the scanning range of 20° to 60°, with CuKα 1.5406 Å radiation.

Electrochemical characterizations were carried out using a conventional three-electrode cell composed of $Ti/IrO_2—Nb_2O_5$ employed as the working electrode, with 1 cm² of exposed geometric area. The Ag/AgCl (saturated) electrode and Pt plate were used as the reference and counter electrodes, respectively, and H_2SO_4 and K_2SO_4 0.5 mol L^{-1} were employed as supporting electrolyte. The voltammetric experiments were performed in the range of 0.15 to 1.15 V, with a scan rate of 50 mVs^{-1}.

The morphology factor for the anode obtained was determined by the methodology proposed by Da Silva et al. [29]. CV measurements were performed in the capacitive potential range of 0.3 to 0.5 V vs $Ag/AgCl/KCl_{sat}$, where the electrical double layer was charged to allow the certification of the capacitive current density (*jc*) - which is considered the final 20% of the capacitive potential range (which was 0.46 V in this case).

To evaluate the electronic properties of the electrodes, impedance spectroscopy measurements were carried out using 0.5 mol L^{-1} K_2SO_4 as supporting electrolyte at 1.10 V, from 10 kHz down to 10 mHz, with perturbation of 10 mV_{rms}. In addition, Mott-Schottky curves were gen-

erated from the impedance data at different polarization potentials to evaluate the major charge carriers of the materials. Electrochemical measurements were carried out using AUTOLAB potentiostat/galvanostat PGSTAT-30 (EcoChemie, Utrecht, Netherlands) with FRA2 module and NOVA 2.1 software. The photocatalytic activity of the proposed electrodes was measured using Vapour Metallic Lamp, 150 W (HQI-TS Osram).

2.4. Levofloxacin (LFX) degradation assays

The treatment processes, namely, photolysis (pH), electrochemical (EC) method, and photoelectrochemical (PhEC) method, targeted at the degradation of the LFX antibiotic were executed in a glass reactor (150 mL) with the UV–Vis lamp (125 W) positioned in the center. $Ti/IrO_2—Nb_2O_5$ was used as the anode, saturated Ag/AgCl/KCl as the reference electrode, and Pt plate as the auxiliary electrode. The effect of the current density (6.0 and 12.5 mA cm^{-2}) on the degradation of 20 mg L^{-1} LFX was evaluated using 0.5 mol L^{-1} Na_2SO_4 solution for 90 min. All experiments were performed under magnetic stirring. Aliquots of the LFX solutions were taken at a regular interval to follow the progress of the degradation assays; the aliquots were filtered using 0.45 μm filter and employed for further analysis. To investigate the effect of the water matrix and the real applicability of the system developed, the $Ti/IrO_2—Nb_2O_5$ electrode was used for the degradation of LFX (20 mg L^{-1}) spiked in a real natural water matrix (river water). The real river water was collected from the University of São Paulo (USP) - Brazil (−21.999120345468054, −47.87738515302277), and the main characteristics are shown in Table 1. The addition of sulfate salt (by K_2SO_4) to the real water matrix was conducted before degradation experiments to increase the electroconductivity.

2.5. Specific energy consumption

The specific energy consumption per unit TOC mass (EC_{TOC}) was calculated for the PhEC process applied at different current densities using Eq. (1) below:

$$EC_{TOC}\left(kWh\,g^{-1}\,TOC^{-1}\right) = \left(\frac{E_{cell} \times I \times t + P \times t}{V_s \times (\Delta TOC)_{exp}}\right) \quad (1)$$

Where E_{cell} is the average cell potential (V), I is the applied current (A), t is the electrolysis time (h), P is the nominal power of the UV–Vis lamp (W), V_s is the solution volume (L), and $(\Delta TOC)_{exp}$ is the TOC removal rate (g L^{-1}).

2.6. Analytical methods

The analysis related to LFX removal was conducted by high-pressure liquid chromatography (HPLC) using Shimadzu Prominence HPLC, model LC-20AT (UV-DAD detector) and Phenomenex® Luna C18 column (250 mm × 4.6 mm, 5 μm) at 40 °C. The mobile phase employed consisted of acetonitrile and water with 0.5% formic acid (50/50) and elution mode at 0.5 mL min^{-1}. The injection volume applied was 20 μL and the LFX concentration was detected at 295 nm, with a retention time (t_r) of 4.0 min.

The concentration of total organic carbon (TOC) was monitored using Shimadzu TOC-Vcpn equipment; this was done by collecting 10 mL of the final and initial solutions. The analysis of TOC was carried out after mixing a diluted volume of the treated sample with 6 mol L^{-1} phosphoric acid and sodium thiosulphate (30% m/v) solutions aimed at determining the inorganic and total carbon concentrations, respectively. TOC is obtained by subtracting the value of inorganic carbon (IC) from that of total carbon(TC) (i.e.,TOC = TC – IC); the value obtained helps to measure the CO_2 generated.

To assess the effect of oxidizing species on the photoelectrochemical degradation of LFX, photoelectrolysis tests were performed under the following quenching conditions, with the addition of equimolar amounts of the materials (5 mmol L^{-1}): tert-butanol (t-BuOH), methanol (MeOH), formic acid (FA), benzoquinone (BQ) and silver nitrate ($AgNO_3$) for •OH, $SO_4^{\bullet-}$, h^+, $O_2^{\bullet-}$ and e^-, respectively.

Table 1
. Characteristics of the real river water used in the present study.

Parameters	Value
Na^+ (mg L^{-1})	1.08 ± 0.014
Ca^{2+} (mg L^{-1})	1.34 ± 0.081
Mg^{2+} (mg L^{-1})	0.832 ± 0.04
Cl^- (mg L^{-1})	0.09 ± 0.015
NO_2^-(mg L^{-1})	0.30 ± 0.024
SO_4^{2-} (mg L^{-1})	0.65 ± 0.120
TOC (mg L^{-1})	1.49 ± 0.021
Conductivity (μS cm^{-1})	5.06 ± 0.019
pH	6.97

3. Results and discussion

3.1. Morphological characterization

Fig. 1a shows the SEM image of the $Ti/IrO_2—Nb_2O_5$ electrode obtained by modified Pechini method. One will observe that the $Ti/IrO_2—Nb_2O_5$ film exhibits a considerable number of flaws and cracks which are an intrinsic feature of the method [30]. Furthermore, it is possible to perceive, with the help of mapping images, good coverage and homogeneous dispersion of the different oxides. Fig. 1b shows XRD patterns of the $Ti/IrO_2—Nb_2O_5$ electrode, where one can observe the presence of IrO_2 (green symbols) and Nb_2O_5 (blue ymbols) on the mixed oxides film. The assignment of the peaks to the oxide diffractograms was performed using the ICSD Database. One can possibly observe the characteristic peak of IrO_2 (PDF Card No. 15–0870) in rutile-like structure and the peaks series that are typically characteristic of an orthorhombic Nb_2O_5 (PDF Card No. 30–0873). Additional peaks related to the titanium support can also be identified; these peaks occur due to the penetration of X-ray through the thin oxide surface.

3.2. Electrochemical characterization

Fig. 2a-b shows the cyclic voltammograms obtained for the $Ti/IrO_2—Nb_2O_5$ electrode in 0.5 mol L^{-1} K_2SO_4 and H_2SO_4 as supporting electrolytes, at scan rate (v) of 50 mV s^{-1}. Looking at Fig. 2a-b, one will notice the presence of two oxidation (I/II) and reduction (III/IV) processes in the voltammograms of $Ti/IrO_2—Nb_2O_5$ in the acid medium (Fig. 2a). These processes that occur at 0.60 and 0.95 V correspond to the surface transitions of Ir, which consist of Ir (III)/Ir(IV) and Ir(IV)/Ir(V), and the redox pair [31]. In addition, the presence of these redox processes can be attributed to the kind of oxides obtained from the preparation of the electrode, which, in essence, may appear as a direct consequence of the method applied and the preparation conditions involved [32]. On the other hand, in the K_2SO_4 neutral medium, one will notice that these peaks are no longer evident. As well known in the literature, the redox potential is a measure of the activity of electrons, and it is related to the pH. Thus, for these iridium-based electrodes, a change of the pH to 6 provokes a corresponding change in the redox peak potential. It is also worth noting that in presence of sulfate anions the increase in the pseudocapacitive behavior is observed which also can contribute to overlap the oxidation and reduction peaks, that presents a lower current.

The photocurrent property of the modified electrodes was evaluated in both dark conditions (in the absence of irradiation) and under irradiation with UV–Vis lamp (Fig. 3a). The results obtained from this analy-

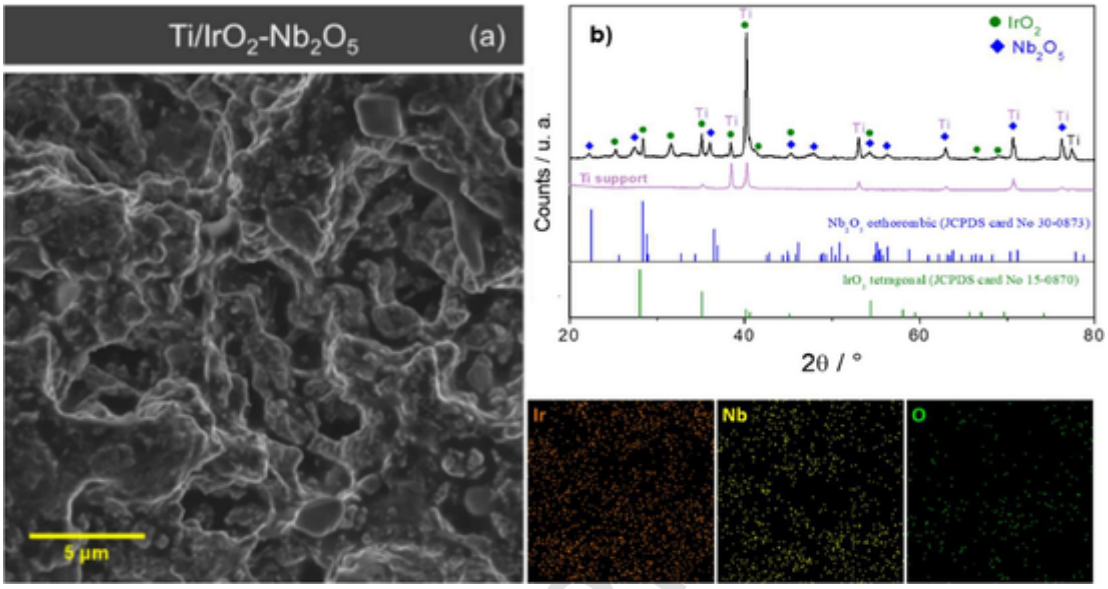

Fig. 1. SEM micrographs, with element mapping in details (a) and (b) X-ray diffractograms of the Ti/IrO_2—Nb_2O_5 electrode.

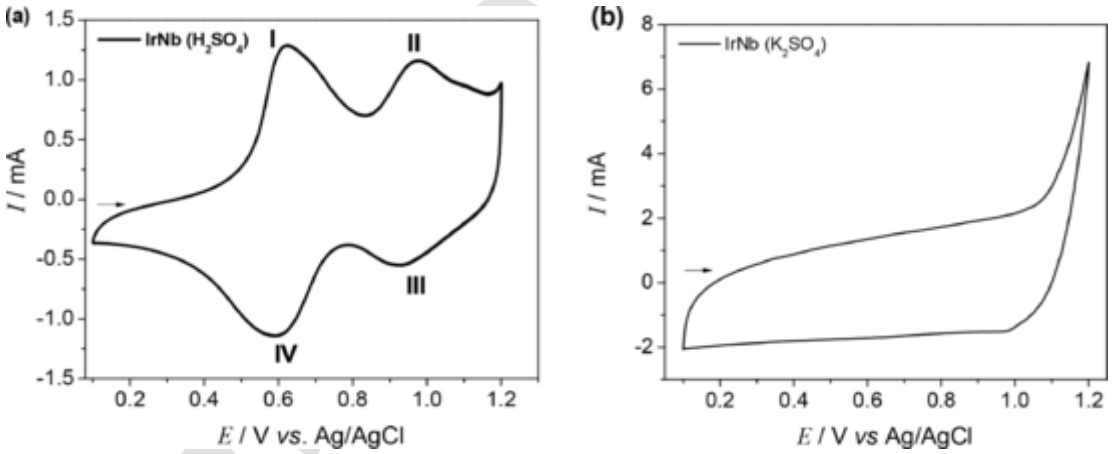

Fig. 2. Cyclic voltammograms of the Ti/IrO_2—Nb_2O_5 electrodes obtained from the application of (a) 0.5 mol L^{-1} H_2SO_4 and (b) 0.5 mol L^{-1} K_2SO_4 as supporting electrolytes; scan rate (v) = 50 mV s^{-1}.

sis showed a slight increase in the current below 0.95 V and a non-negligible increase mainly at around 1.1 V; in view of that, the potential of 1.1 V was chosen for the conduct of the electrochemical impedance spectroscopy analysis as this was the electrode potential employed in the electro and photoelectrodegradation processes. The impact of irradiation can be observed in the Nyquist plots shown in Fig. 3b; these plots represent the magnitude of impedance of the electrodes polarized at the chosen potential [33]. In the present study, Nyquist plots were obtained at the anodic oxygen evolution reaction (OER) onset potential (determined as 1.1 V vs Ag/AgCl). Looking at the Nyquist plots, the spectra can be found to be characterized by a well-developed semi-circle, which is typical for OER charge transfer processes. It should be noted that the size of the semi-circle decreases when the electrodes are subjected to illumination; this outcome points to a significant improvement in the process involving the charge transfer in OER [33–34]. The values obtained by adjusting the data using the equivalent circuit represented in the inset of Fig. 3b are summarized in Table 2.

A careful analysis of the values obtained from the adjustment of the data shows that there was a 50% decrease in the resistance to charge transfer when the Ti/IrO_2—Nb_2O_5 electrode was irradiated with UV–Vis light; this outcome shows that the anode exhibited a better performance under illumination r than in the dark. Moreover, due to the charge carrier movement, there was also a non-negligible improvement in the circuit parameters related to the properties of the electrode material - mainly its resistance. The real capacitance values were obtained by converting the constant phase element (CPE) data and the n associated with this circuit element and showing that the charge separation observed both at the electrode interface in the double layer and internally is attributed to the different movements of the charge carriers.

Fig. 3c shows the band diagram scheme assembled based on information obtained by Mott-Schottky and Uv-Vis spectra by diffuse reflectance, which is better described in the Supplementary Information. Herein, it is possible to observe that the hybrid materials possibly gave rise to a heterojunction with a relative band position intermediate between the pure materials. Furthermore, such a diagram will guide future discussions.

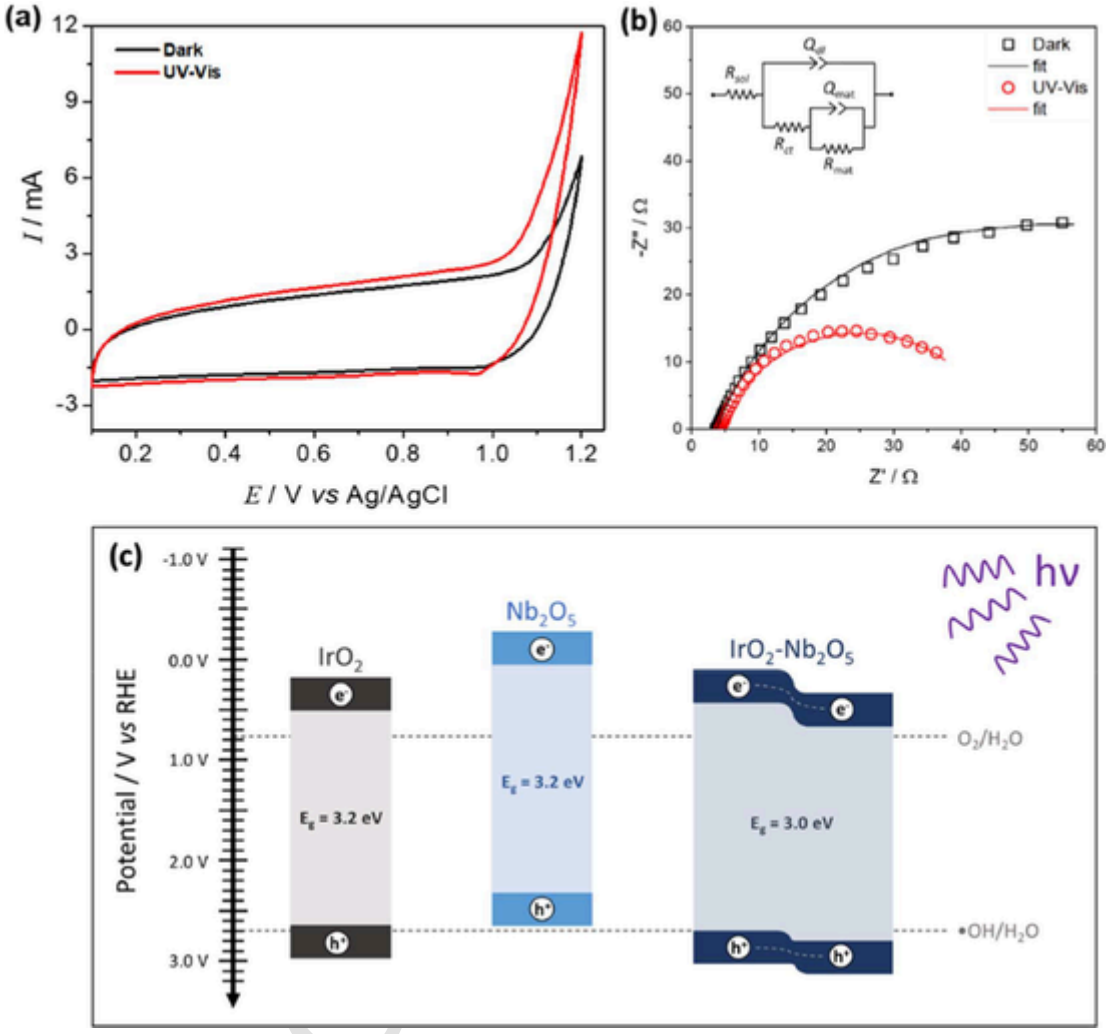

Fig. 3. Cyclic voltammograms obtained for the Ti/IrO_2—Nb_2O_5 electrode using 0.5 mol L^{-1} K_2SO_4 as supporting electrolyte in the presence and absence of UV–Vis illumination, with $\upsilon = 50$ mV s^{-1} (a); Nyquist plots (b); Band diagram scheme (c).

Table 2
. Impedance data obtained from the adjustment of the parameters.

Conditions	R_{ct} (Ω)	C_{dl} (mF)	R_{mat} (Ω)	C_{mat} (μF)	K_{ct} (s^{-1})	χ^2
Dark	85.0	12.1	0.156	30.1	9.69×10^{-2}	4.35×10^{-4}
UV–Vis	41.2	9.74	0.0514	24.7	3.14×10^{-1}	7.44×10^{-4}

One remarkably important parameter that needs to be evaluated in a catalyst material meant for electrochemical applications is its specific surface area. When one varies the potential of an electrode at a given scan rate, the measured electrical current is found to be directly proportional to the electrode surface exposed to the electrolyte [35]. With the dramatic advancement in nanoengineering and the availability of a wide range of synthesis techniques that can be used to obtain mixed oxide-based electrodes, one can increase the surface area of an electrode so that the geometric area of the flat electrode is substantially different from the electrochemically active area. Thus, determining the active surface area of an electrode becomes essentially important when one seeks to evaluate its catalytic performance.

As widely reported in the literature, the electrochemically active surface area (ECSA) can be determined via the application of a wide range of methods [36–37]. In this work, ECSA was measured using cyclic voltammetry, with cycles in the non-faradaic region of potentials (at −0.40 V vs Ag/AgCl) at varying scan rates (5 to 75 mV s^{-1}). The inset in Fig. 4a shows the CVs obtained at the different scan rates investigated. The double layer electrical capacitance (C_{dl}) of 2.78 e^{-1} F cm^{-2} was obtained from the linear slope corresponding to the evolution of the non-faradaic current density at the scan rates investigated - see Fig. 4a. Based on the value of C_{dl} and considering the standard flat area of capacitance (Cs) of 40 μF cm^{-2}, the ECSA of Ti/IrO_2—Nb_2O_5 was estimated from the Eq. (2) below [38–40]:

$$ECSA = \frac{Cdl}{Cs} \quad (2)$$

The results obtained from this calculation showed that the ECSA of the Ti/IrO_2—Nb_2O_5 electrode was approximately 695.0 per ECSA cm^{-2} - see Table 3. For comparison purposes, Sun et al. (2021) obtained ECSA/cm^2 of 287.71 for thermally decomposed IrO_2–containing mixed oxide electrodes - $(Ir_{0.4}Pr_{0.4}Si_{0.2})Ox$ [39]. Xiong et al. (2020) obtained ECSA/cm^2 of 350.0 for $Zr_{0.3}Ir_{0.7}O_2$ electrode which exhibited high catalytic activity [41]. The Ti/IrO_2—Nb_2O_5 electrode prepared in this work recorded about twice the ECSA value obtained in the aforementioned studies; this result points to the outstanding catalytic activity of the proposed Ti/IrO_2—Nb_2O_5 electrode and a greater exposure of its active sites. As mentioned above, the morphology of the Ti/IrO_2—Nb_2O_5 electrode was characterized by a film with several

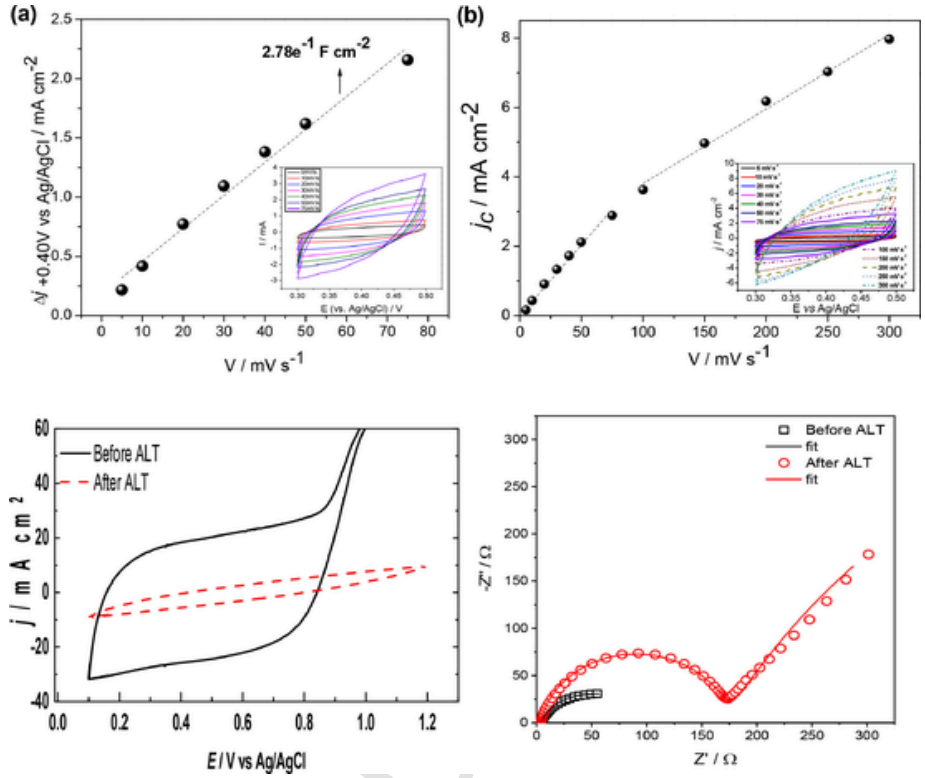

Fig. 4. Relationship between capacitive current density (average) at +0.40 V and different scan rates applied (5 – 75 mV s^{-1}) for the ECSA analysis (a) and variation of capacitive current density (j_c) as a function of scan rate (ν) (5 – 75 mV s^{-1} and 100 – 300 mV s^{-1}) for the morphology factor analysis (b); supporting electrolyte: 0.5 mol L^{-1} K_2SO_4. Cyclic voltammograms obtained for the Ti/IrO_2—Nb_2O_5 electrode before and after accelerated lifetime/stability test using 0.5 mol L^{-1} H_2SO_4 as supporting electrolyte (c); and Nyquist plots using 0.5 mol L^{-1} K_2SO_4 as supporting electrolyte (d), with υ = 50 mV s^{-1}.

Table 3
. Impedance data obtained from the adjustment of the parameters.

Conditions	R_{ct} (Ω)	C_{dl} (mF)	R_{mat} (Ω)	C_{mat} (μF)	K_{ct} (s^{-1})	χ^2
Before ALT	85.0	12.1	0.156	30.1	9.69×10^{-2}	4.35×10^{-4}
After ALT	168	1.16	116×10^{1}	142	5.36×10^{-3}	3.45×10^{-4}

cracks and deformations. Clearly, the presence of these many cracks and deformations in the proposed electrode leads to an increase in its surface area and a resulting increase in its active area compared to electrodes with flatter surfaces. Based on the cyclic voltammograms, one can obtain valuable information regarding the degree of roughness of the electrode surface by calculating the morphology factor [29]. Based on the methodology proposed by Da Silva et al. [29], one can construct a graph correlating the variation in capacitive current density (j_c) with the scan rate (ν) (Fig. 4b). As can be observed, there are two different regions on the graph (a common behavior of highly rough films). These regions can be associated with the reactions that take place on the surface of the electrode at different scan rates; at low scan rates, all the active sites on the electrode surface are noticeably accessible (i.e., both internal and external sites), whereas, at high scan rates, these reactions take place only at the external sites, which are more accessible. Thus, the morphology factor (φ) can be obtained by means of the ratio between the most difficult-to-access region and the easiest-to-access region and the total accessible active sites, as shown in Eq. (1) below, where $C_{d,I,}$ and C_d correspond to internal differential capacitance and total differential capacitance, respectively.

$$\varphi = \frac{C_{d,i}}{C_d} \quad (1)$$

Since φ values vary from 0 to 1, values approaching 0 indicate that the internal sites present negligible contribution to the total capacitance, while values close to 1 point to a significant contribution of the internal active sites on the total capacitance of the electrode. The C_d, $C_{d,i}$ and $C_{d,e}$ and φ values obtained are shown in Table 3.

Based on the results obtained from the calculation of the morphology factor (φ = 0.47), we noted that the active sites on the Ti/IrO_2—Nb_2O_5 electrode are uniformly distributed on the anode surface.

Since mixed metal oxide (MMO) electrodes are required to last for many years when employed in real applications, it is of crucial importance to determine the lifetime of the electrodes obtained through the implementation of accelerated stability tests. In these tests, high current densities are applied, and the potential response is monitored; an abrupt increase in potential indicates the deactivation of the anode. In the present study, the Ti/IrO_2—Nb_2O_5 electrode was subjected to drastic electrolysis conditions (current density: 400 mA cm^2; supporting electrolyte: 0.5 M H_2SO_4), referred to as the accelerated lifetime test (ALT). The results obtained showed that the Ti/IrO_2—Nb_2O_5 electrode lasted 79.5 h under these drastic conditions. To gain a better understanding of the deactivation mechanism, CV and EIS measurements were performed for the electrode after the accelerated lifetime/stability test.

The results obtained showed that the voltammetric charge decreased by 85%; this result shows that the deactivation mechanism of the Ti/IrO_2—Nb_2O_5 electrode occurred via two ways: i) through the detachment of the oxide layer due to the intense generation of oxygen bubbles, and ii) through the formation of an isolating layer of TiO_2 because of the continuous dissolution of RuO_2 species, since 15% of the coating remains on the electrode after deactivation [42]. The deactivation mechanism is commonly related to the morphology of the

coatings since more compact coating prevents the penetration of electrolyte through the surface of the catalytic layer and reaching the Ti substrate. The Nyquist plots obtained for the anodes after deactivation pointed to a significant increase in the semicircle diameter; in other words, there was an expected increase in R_{ct} due to the considerable reduction of the electrocatalytic activity stemming from both the progressive dissolution of ruthenium and the formation of TiO_2 insulating layer. Having a comprehensive understanding of the mechanisms involved in the deactivation of an anode is essentially crucial because the electrocatalytic capacity of the anode is tested over time; this is especially the case when one takes into account the addition of a stabilizing metal oxide (in the present study, Nb_2O_5 plays this role) (Table 4).

3.3. Degradation assays

Fig. 5 shows the% of TOC removal and the decay of LFX concentration at the current density of 12.5 mA cm^{-2} based on the application of the Ti/IrO_2—Nb_2O_5 electrode under the pH, EC and PhEC techniques in 90 min of treatment. In the irradiated process (pH and PhEC), a UV–Vis lamp was employed. The type of treatment process employed was a determining factor when it comes to the efficient removal of the LFX compound. The application of the EC process promoted the lowest LFX degradation rate. Although MMO-type electrodes generally present high catalytic activity when applied for the degradation of organic compounds in electrolysis, in these systems, high current densities are commonly used [15,43]. In our present work, the electrolysis were conducted at relatively lower current densities compared to those applied in studies reported in the literature; the application of lower current densities may have led to a relatively lower generation of reactive oxygen species, which hindered the direct degradation of LFX. In view of that, the EC technique yielded relatively lower LFX degradation rate (<10%) and EC kinetic constant (0.0010 min^{-1}). Furthermore, EC did not promote antibiotic mineralization, as observed in the% TOC removal – see Fig. 5b.

On the other hand, both the pH and PhEC techniques promoted total degradation of the LFX antibiotic after 90 min of treatment. The PhEC technique recorded a slightly higher LFX degradation rate compared to the pH technique. The apparent LFX degradation rates obtained from the application of the techniques were 0.1209 min^{-1} and 0.0816 min^{-1} for PhEC and pH, respectively; this result points to the synergistic effect between UV–Vis irradiation and the current density applied to the Ti/IrO_2—Nb_2O_5 electrode. Although the pH process also promoted the total degradation of the LFX antibiotic in 90 min, the% TOC removal obtained from the application of this process (50%) was twice the value obtained for the pH process (24%); essentially, this result shows that although light irradiation promotes the breakdown of the molecule of interest, it may also lead to the formation of recalcitrant intermediates, which are difficult to remove. Similar behavior was reported by Goulart et al. (2021) when the authors employed a photoactive Ti/MMO/ZnO anode for LFX degradation; according to the authors, although the application of the pH treatment process promoted a high LFX degradation rate (67%) after UVC light irradiation, the process promoted only 6.0% TOC removal at the end of the treatment. In this same work, the authors showed that the application of the PhEC process with Ti/MMO/ZnO electrode promoted 100% degradation of LFX, with 38% TOC removal; furthermore, relatively less degradation products were formed under the PhEC process compared to the pH process [43]. Several studies reported in the literature have shown that the application of the PhEC process results in fast and highly efficient removal of organic compounds, with the formation of few organic intermediates and short chain acids of easy mineralization [44–45]. Thus, the application of the PhEC process for the treatment of organic compounds generally leads to higher TOC removal rates compared to the EC and pH processes.

To evaluate the effect of current density on LFX removal, the proposed Ti/IrO_2—Nb_2O_5 electrode was evaluated based on the application of the PhEC process at the current density of 12.5 mA cm^{-2} and at a lower current density (6.0 mA cm^{-2}) in 90 min. As can be seen in Fig. 6a, the application of both current densities

(12.5 mA cm^{-2} and 6.0 mA cm^{-2}) led to similar results in terms of the decay of LFX concentration as a function of time, where the compound was found to have been completely degraded at the end of the treatment. It is worth noting however that the application of the PhEC process at the current density of 6.0 mA cm^{-2} promoted a 15% increase in TOC removal compared to the PhEC process applied at 12.5 mA cm^{-2} in 90 min of treatment – see Fig. 6b. At lower current densities, one ob-

Table 4
. Results related to the electrochemically active surface area (ECSA), roughness factor and total differential capacitance (Cd,t), external capacitance (Cd,e) and internal capacitance (Cd,i), and the accelerated lifetime test (ALT) for the Ti/IrO_2—Nb_2O_5 anode.

Electrode	ECSA/cm^2	$C_{d,t}$ (F)	$C_{d,e}$ (F)	$C_{d,I}$ (F)	ϕ	ALT	q^*(before ALT)	q^*(after ALT)
Ti/IrO_2—Nb_2O_5	695.0	40.82	21.48	19.34	0.47	79.5	1681.5	254

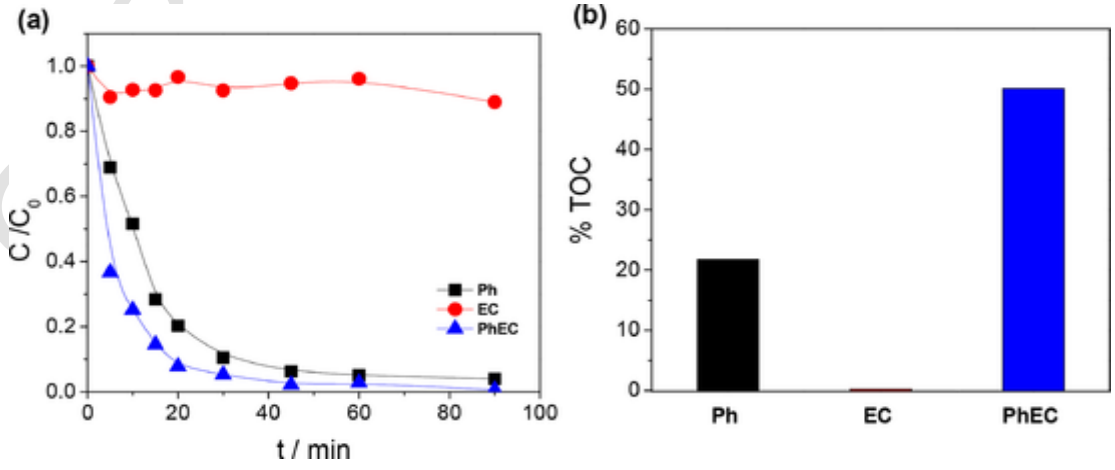

Fig. 5. Effect of the application of photolysis (pH), electrolysis (EC) and photoelectrolysis (PhEC) on the degradation of 20 mg L^{-1} of LFX in 0.5 mol L^{-1} of K_2SO_4 using Ti/IrO_2—Nb_2O_5 electrode (a) and TOC removal (b). Conditions applied: j = 12.5 mA cm^{-2}; time/duration = 90 min.

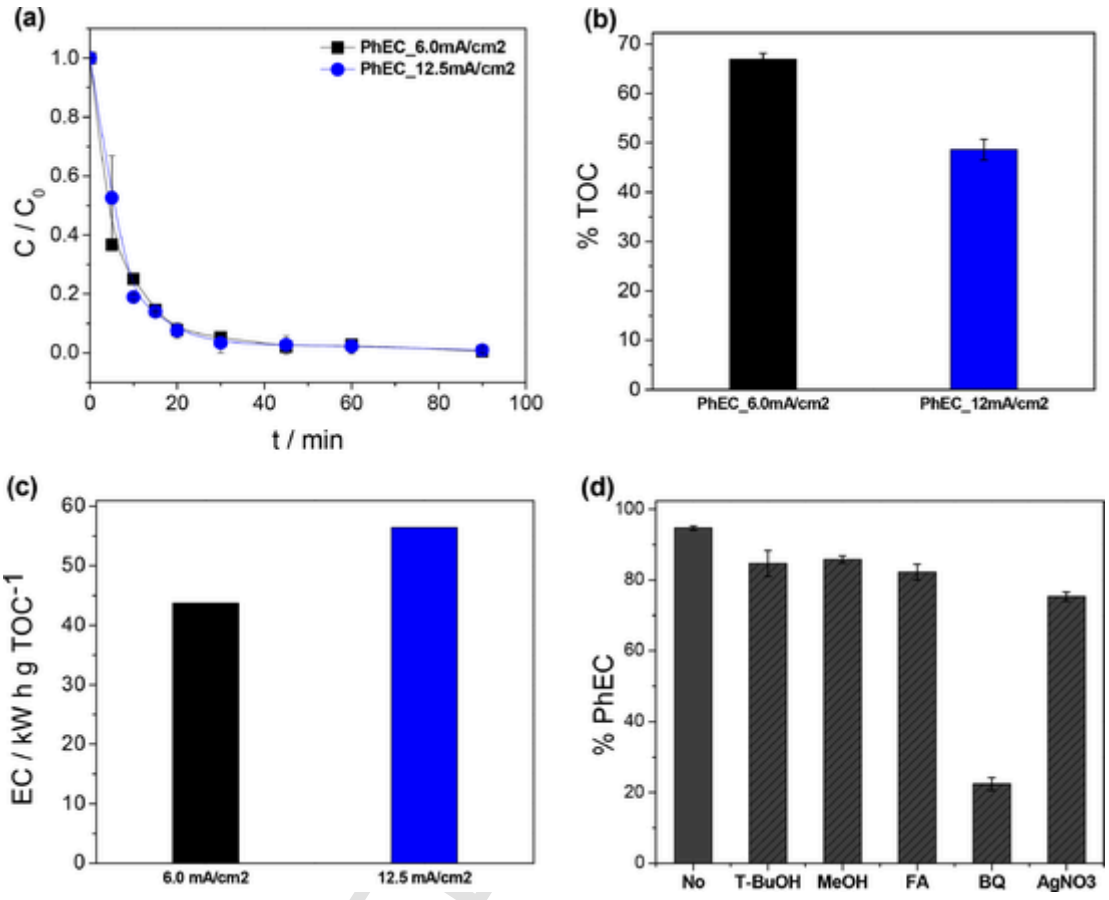

Fig. 6. Effect of current density (j = 6.0 and 12.5 mA cm^{-2}) on the degradation of 20 mg L^{-1} of LFX with electrolysis time, based on the application of the photo-electrocatalytic treatment using Ti/IrO_2—Nb_2O_5 electrode in 0.5 mol L^{-1} K_2SO_4 (a), and TOC removal (b); energy consumption (in kWh per gram of TOC removed) (EC) at different current densities (c); and the analysis of the effects of quenching agents (5.0 mmol L^{-1}) on the PhEC of LFX – HO•(T-BuOH), SO_4•−(MeOH), h^+ (FA), O_2•− (BQ) and e^- ($AgNO_3$) (d).

serves a decrease in the formation of oxygen on the electrode surface [46], and this tends to increase the exposure of the catalyst sites of the Ti/IrO_2—Nb_2O_5 electrode, leading to an increase in the antibiotic removal rates. As can be observed in Fig. 6c, the application of the current density of 6.0 mA cm^{-2} resulted in a relatively lower specific energy consumption per unit mass TOC (EC_{TOC}) – 43.7 kWh g-TOC^{-1}, compared to the current density of 12.5 mA cm^{-2} (56.4 kWh g-TOC^{-1}). Thus, 6.0 mA cm^{-2} was chosen as the optimal current density for the conduct of the PhEC treatment using the /IrO_2—Nb_2O_5 electrode.

Some trapping agents were employed in order to help distinguish the free radical species derived from the application of the Ti/IrO_2—Nb_2O_5 electrode in the PhEC advanced oxidation process for the degradation of LFX. Thus, in essence, the trapping/quenching agents were primarily employed in order to determine the mechanisms involving the degradation of LFX. As can be seen in Fig. 6b, the trapping/quenching agents (also referred to as scavengers) capture HO•, SO_4•−, h^+, O_2•− and e^-using (T-BuOH), (MeOH), (FA), (BQ) and ($AgNO_3$), respectively. For illustration purposes, methanol (MeOH) was used as a quenching agent for HO• and SO_4•−. MeOH reacts with HO• and SO_4•− at rates of 1.0 × 10^9 and 2.5 × 10^7 M^{-1} s^{-1}, respectively [47,48]. Isopropanol (T-BuOH) was added into the mixture as HO• scavenger [48]. Finally, BQ was used to capture superoxide anion radical O_2•−. FA was used as h^+ trapping agent, while $AgNO_3$ was used to capture e. As demonstrated in Fig. 6d, the addition of T-BuOH, MeOH, FA, BQ and $AgNO_3$ into the reaction medium led to a decrease in LFX removal from 100% to 88%, 87%, 80%, 20% and 75%, respectively; this outcome points to the production of HO•, SO_4•−, h^+ O_2•− and e^-. O_2 single electron reduction process (Eq.(2)) has the potential to produce O_2•−. Indeed, O_2•- is produced according to the reaction described in Eq. (3). O_2•− in turn generates $^1O_2$ (Eq. (2) – (3)).The addition of excess T-BuOH into the medium leads to a decrease in LFX removal from 100% to 88%; this result is clearly indicative of the presence of HO• within the process. The HO• present in the treatment process mainly originates from the reactions in Eq. (4) and (5) below [41]. Thus, the degradation of LFX in the PhEC process involves several different routes; these routes include the reactions involving radical species (SO_4•−, HO•, and O_2•−) and those involving non-radical ($^1O_2$) species.

$$O_2 + e^- \rightarrow O_2^{\bullet -} \quad (2)$$

$$S_2O_8^{2-} + HO_2^- \rightarrow SO_4^{2-} + SO_4^{\bullet -} \ldots + \ldots O_2^{\bullet -} + H^+ \quad (3)$$

$$H_2O + \text{MeOx electrode} \rightarrow \text{MeOx electrode}(HO^{\bullet}) + H^+ + e^- \quad (4)$$

$$SO_4^{\bullet -} + H_2O \ldots \rightarrow H^+ + SO_4^{2-} + HO^{\bullet} \quad (5)$$

Although the LFX oxidation mechanism involves different species of radicals formed during PhEC with Ti/IrO_2—Nb_2O_5, according to the scavenger experiments, the superoxide radical was the one that had the greatest influence on the treatment. The formation of O_2•− may be related to the galvanostatic nature of the treatment, which promotes the formation of a large amount of O_2 at the photoanode. During PhEC, electrons from the semiconductor surface reduce O_2 to superoxide, this species being mainly responsible for the degradation of LFX. Due to the large amount of superoxide formed, the contribution of other oxidizing species to the photocatalytic process can be inhibited. It is known that a

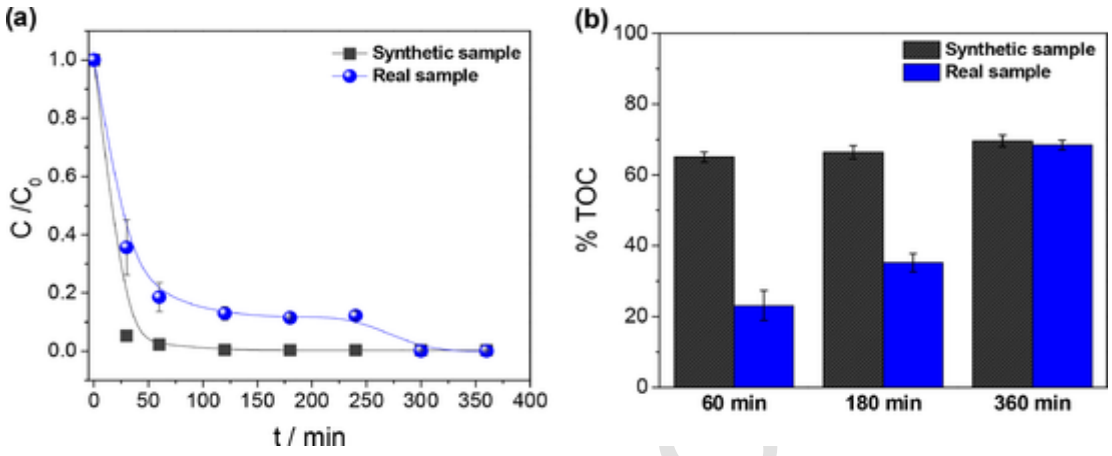

Fig. 7. Results obtained from the thorough photoelectrocatalysis (PhEC) treatment conducted based on the application of the proposed Ti/IrO_2—Nb_2O_5 electrode for the degradation of 20 mg L^{-1} of LFX in 0.5 mol L^{-1} K_2SO_4 (synthetic sample) and in real sample (a); TOC removal in synthetic sample and real sample (b). Conditions applied: j = 6.0 mA cm^{-2}; treatment time: 360 min.

good photocatalyst in the presence of O_2, in addition to forming hydroxyl radicals, also promotes the formation of $O_2^{\bullet-}$, with high oxidizing power, through the donation of electrons [49].

3.4. Thorough degradation of LFX in synthetic and real water matrices

The aqueous matrix used in the degradation process plays a very important role in terms of the efficiency of photoelectrocatalysis. With that in mind, in order to investigate the application potential of the treatment process developed in the present study, river water samples spiked with 20 mg $L^{-1}$of LFX (real sample) were subjected to PhEC treatment using the Ti/IrO_2—Nb_2O_5 electrode, under previously optimized conditions for 360 min, and the results obtained were compared to those of the PhEC treatment process executed in 0.5 mol L^{-1} K_2SO_4 (synthetic sample) – see Fig. 7. As can be observed in Fig. 7a, the degradation of LFX in the real river water sample occurred at a relatively slower rate compared to the synthetic water sample. In 30 min of treatment, for example, about 95% of the pollutant was removed from the synthetic sample, whereas only 72% was removed from the real sample; also, a PhEC treatment period of approximately 300 min was required to obtain a total degradation of the compound in the real aqueous matrix. Furthermore, for the synthetic sample, TOC removal rate of around 70% was obtained in 60 min of PhEC treatment, whereas a PhEC treatment period of 360 min was required to obtain this same TOC removal rate in the real sample.

Kronka et al. (2022) also observed a decrease in the rate of organic pollutants removal when they applied EAOPs for the treatment of real aqueous samples [50]. In the aforementioned study, the authors employed the photoelectron-Fenton process with gas diffusion electrode (GDE) based on AuNPs, ZrO_2 and carbon black for the degradation of carbaryl pesticide (CBR) in both synthetic and real urban sewage samples. According to the authors, CBR degradation occurred 1.6 times faster in the synthetic medium compared to the real sample; furthermore, the authors also observed the same trend in terms of TOC removal, where about 82% and 71% of TOC was removed in the synthetic and real urban sewage samples, respectively, after 60 min of electrolysis [50]. Interestingly, Frontistis et al. (2017) reported to have obtained different results when they compared the removal of the pollutant ethyl paraben in sulfate medium and real effluent medium based on the application of electrolysis with DDB electrodes; the authors observed a relatively faster removal of the organic compound in the real effluent matrix compared to the sulfate medium [51]. The authors of the aforementioned study attributed the results they obtained to the formation of other oxidizing species, in addition to hydroxyl radicals and sulfate ions, which were generated from the various anions present in the wastewater [51].

Regarding photocatalytic systems, some studies have reported that the photocatalytic efficiency of these systems can significantly decrease when they are applied for pollutants degradation in the presence of inorganic ions [52–53]. This behavior is mainly attributed to the adsorption of ions on the surface of the photocatalyst, in addition to the elimination of oxidizing radicals by salts and organic matter present in real water matrices [54–55]. Furthermore, the presence of natural organic matter (NOM), derived from the decomposition of plants, for example, can compete with LFX for oxidants, and this may explain the decrease in the rate of degradation of this compound in real water sample (river water). Although the degradation and mineralization rate of LFX was found to be slower in the real sample, it is noteworthy that the application of the PhEC treatment process using the Ti/IrO_2—Nb_2O_5 electrode resulted in LFX removal efficiency similar to that obtained for the synthetic sample at the end of the treatment process; this result clearly points to the application potential of proposed technique when applied for LFX treatment in real samples.

4. Conclusion

Based on the results obtained in this study, we present the following conclusions:

- The Ti/IrO_2—Nb_2O_5 electrode, which was successfully prepared in this study using a quick, simple synthesis procedure (modified Pechini method), exhibited excellent photocatalytic properties.
- Apart from the high stability proven by the lifetime tests conducted, the Ti/IrO_2—Nb_2O_5 electrode exhibited a relatively higher electroactive area (calculated by means of ECSA) compared to stable mixed oxide-based electrodes previously reported in the literature.
- The results obtained from the degradation assays conducted in the study showed that the application of the Ti/IrO_2—Nb_2O_5 electrode under the PhEC process led to more efficient LFX removal and mineralization (70%) compared to the single EC (6%) and pH treatment processes (20%); this outcome points to the great synergistic effect between the light incidence and the electrode polarization.
- Furthermore, the application of lower current densities in the Ti/IrO_2—Nb_2O_5–based PhEC treatment process led to the

enhancement of LFX degradation, with low energy consumption. By studying the action of the scavengers, the degradation process involved in the PhEC treatment technique was clearly elucidated. The findings of the study showed that the application of the PhEC process led to the formation of different radical species, including $SO_4^{\bullet-}$, HO•, and $O_2^{\bullet-}$, as well as photogenerated species – such as the e^-/h^+ pair, on the electrode surface; this result points to the complex process involving the degradation of LFX.

- Finally, the application of the $Ti/IrO_2—Nb_2O_5$ anode –based PhEC treatment technique promoted high rates of LFX removal in both synthetic and real natural water samples; this result points to the versatility of the electrode and the applicability of this system for the effective treatment of organic pollutants in environmentally relevant water matrices.
- Considering the high efficiency of $Ti/IrO_2—Nb_2O_5$ in the removal of organic pollutants by applying current density, LFX degradations will be further investigated under controlled potential, since in this condition the oxidation of water to oxygen can be avoided, favoring the removal of TOC, resulting in a decrease in the energy consumption of the treatment.

Declaration of Competing Interest

The authors declare that they have no known competing financial interests or personal relationships that could have appeared to influence the work reported in this paper.

Acknowledgements

The authors gratefully acknowledge the assistance provided by FAPESP (Grants #2014/50945–4, #2016/08760–2, #2017/10118–0, #2018/09761–8 and #2020/02743–4), FAPESP/SHELL (#2017/11986–5), FAPESP/CEPID (#2013/07296–2), CNPq (#303759/2014–3, #303943/2021–1 and #116926/2022–8) and CAPES finance code 001 in support of this research. We would also like to thank the Center for Development of Functional Materials (CDMF) for granting us access to their facilities.

Supplementary materials

Supplementary material associated with this article can be found, in the online version, at doi:10.1016/j.electacta.2023.143586.

References

[1] A. Nikolaou, S. Meric, D. Fatta, Occurrence patterns of pharmaceuticals in water and wastewater environments, Anal. Bioanal. Chem. (2007), https://doi.org/10.1007/s00216-006-1035-8.

[2] G.O.S. Santos, L.A. Goulart, P.J. Cordeiro-Junior, I. Sánchez-Montes, M.R.V. Lanza, Pharmaceutical contaminants: ecotoxicological aspects and recent advances in oxidation technologies for their removal in aqueous matrices, J. Environ. Chem. Eng. (2022), https://doi.org/10.1016/j.jece.2022.108932.

[3] K. Samal, S. Mahapatra, M.H. Ali, Pharmaceutical wastewater as Emerging Contaminants (EC): treatment technologies, impact on environment and human health, Energy Nexus (2022), https://doi.org/10.1016/j.nexus.2022.100076.

[4] Patricia Pereira, Magalı Rey-Campos, Antonio Figueras, Beatriz Novoa, An environmentally relevant concentration of antibiotics impairs the immune system of zebrafish (Danio rerio) and increases susceptibility to virus infection, Front. Immunol. (2023), https://doi.org/10.3389/fimmu.2022.1100092.

[5] C. Wu, C. Kuo, D. Dong, Y.L. Lin, Removal of sulfonamides from wastewater in the UV/TiO_2 system: effects of pH and salinity on photodegradation and mineralization, Water Sci. Technol. (2019), https://doi.org/10.2166/wst.2019.053.

[6] Carlos A. Martínez-Huitle, Manuel A. Rodrigo, Ignasi Sirés, Onofrio Scialdon, A critical review on latest innovations and future challenges of electrochemical technology for the abatement of organics in water, Appl. Catal. B Environ. (2023), https://doi.org/10.1016/j.apcatb.2023.122430.

[7] Efraím A Serna-Galvis, Karen E Berrio-Perlaza, Ricardo A Torres-Palma, Electrochemical treatment of penicillin, cephalosporin, and fluoroquinolone antibiotics via active chlorine: evaluation of antimicrobial activity, toxicity, matrix, and their correlation with the degradation pathways, Environ. Sci. Pollut. Res. (2017), https://doi.org/10.1007/s11356-017-9985-2.

[8] P. Ball, Efficacy and, Safety of Levofloxacin in the Context of Other Contemporary Fluoroquinolones: a Review, Curr. Ther. Res. Clin. Exp. (2003), https://doi.org/10.1016/j.curtheres.2003.11.003.

[9] Roman Hirsch, Thomas Ternes, Klaus Haberer, Karl-Ludwig Kratz, Occurrence of antibiotics in the aquatic environment, Sci. Tot. Env. (2023) 4053061, https://doi.org/10.1016/j.curtheres.2003.11.003.24944413.

[10] S.V. Blokhina, A.V. Sharapova, M.V. Ol'khovich, Volkova TV, G.L Perlovich, Solubility, lipophilicity and membrane permeability of some fluoroquinolone antimicrobials, Eur. J. Pharm. Sci. (2016), https://doi.org/10.1016/j.ejps.2016.07.016.

[11] M. Shueai Yahya, N. Beqqua, I. Haji, M. El Karbane, H. Chakchak, I. Warad, A. Zarrouk, G. Kaichouh, Optimization of the Electro-Fenton Process for the elimination of oxytetracycline antibiotic from water: degradation Mineralization kinectics, Anal. Bioanal. Electrochem. (2023), https://doi.org/10.22034/ABEC.2023.704565.

[12] Komissarova Alena, Removal of pharmaceutical micropollutants from real wastewater matrices by means of photochemical advanced oxidation processes: a review, J. Water Process Eng. (2023), https://doi.org/10.1016/j.jwpe.2023.103727.

[13] Jaesang Lee, Urs von Gunten, Jae-Hong Kim, Persulfate-Based Advanced Oxidation: critical Assessment of Opportunities and Roadblocks, Environ. Sci. Technol. (2020), https://doi.org/10.1021/acs.est.9b07082.

[14] Lorena A. Goulart, Angela Moratalla, Marcos R.V. Lanza, Cristina Saez, Manuel A. Rodrigo, Photoelectrocatalytic treatment of levofloxacin using Ti/MMO/ZnO electrode, Chemosphere (2021), https://doi.org/10.1016/j.131303.

[15] Carlos H.M. Fernandes, Marcelo M. Yamasaki, Fernando L. Silva, Vanessa M. Vasconcelos, Robson S. Rocha, Marcos R.V. Lanza, Evandro L.Dall'Óglio e Ailton J. Terezo, Tratamento eletroquímico de efluente da produção de biodiesel usando um eletrodo de Ti/IrO_2-Nb_2O_5, Quim, Nov (2018), https://doi.org/10.21577/0100-4042.20170163.

[16] Ailton J. Terezo, Ernesto C. Pereira, Preparation and characterisation of Ti/RuO_2 anodes obtained by sol-gel and conventional routes, Mater. Lett. (2002), https://doi.org/10.1016/S0167-577X(01)00504-3.

[17] S. Choi, W.I. Choi, J.S. Lee, C.H. Lee, M. Balamurugan, A.D. Schwarz, Z.S. Choi, H. Randriamahazaka, K.T. Nam, A Reflection on Sustainable Anode Materials for Electrochemical Chloride Oxidation, Adv. Mater. (2023) 2300429, https://doi.org/10.1002/adma.202300429.

[18] Hanyang Li, Yuexin Xu, Ning Lv, Qiuyitong Zhang, Xiaolian Zhang, Zijie Wei, Yadong Wang, Haolin Tang, Hongfei Pan, Ti-Doped SnO_2 Supports IrO_2 Electrocatalysts for the Oxygen Evolution Reaction (OER) in PEM Water Electrolysis, Sustain. Chem. Eng. (2023), https://doi.org/10.1021/acssuschemeng.2c06368.

[19] S. Wang, M. Wang, Y. Zhang, H. Wang, H. Fei, R. Liu, H. Kong, R. Gao, S. Zhao, T. Liu, Y. Wang, M. Ni, F. Ciucci, J. Wang, Metal Oxide-Supported Metal Catalysts for Electrocatalytic Oxygen Reduction Reaction: characterization Methods, Modulation Strategies, and Recent Progress, Small Methods (2023) https://doi.org/10.1002/smtd.202201714, Epub ahead of print. PMID: 37029582.

[20] Wei Zhang, C. Jinfa, Y. Yang, Strong precious metal–metal oxide interaction for oxygen reduction reaction: a strategy for efficient catalyst design, Sus. Mat. (2023), https://doi.org/10.1002/sus2.108.

[21] S. Thanka Rajan, J. Senthilnathan, A. Arockiarajan, Sputter -coated N-enriched mixed metal oxides (Ta_2O_5-Nb_2O_5-N) composite: a resilient solar driven photocatalyst for water purification, J. Hazard. Mater. (2023), https://doi.org/10.1016/j.jhazmat.2023.131283.

[22] L. Xia, S. Dong, J. Xin, Kaixuan Gui, Peitao Hu, Yongshuai Xie, Dongdong Yang, Xinghong Zhang, Yanchun Zhou, Fabrication of multi-anionic high-entropycarbonitride ultra-high temperature ceramics by a green and low-cost process with excellent mechanical properties, Sciopen (2020), https://doi.org/10.26599/JAC.2023.9220755.

[23] Gustavo H.M. Gomes, Sunday J. Olusegun, José B. Gabriel, Rayssa C.V. Costa, Nelcy D.S. Mohallem, The role of crystalline Nb_2O_5 nanoparticles for enhanced dye adsorption and photodegradation, Ceram. Int. (2023), https://doi.org/10.1016/j.ceramint.2022.10.126.

[24] Yuanzhi Hong, Changsheng Li, Guangyi Zhang, Yadong Meng, Bingxin Yin, Yong Zhao, Weidong Shi, Efficient and stable Nb2O5 modified g-C_3N_4 photocatalyst for removal of antibiotic pollutant, Chem. Eng. J. (2016), https://doi.org/10.1016/j.cej.2016.04.092.

[25] Saad Ullah Khan, Joao Angelo Lima Perini, Sajjad Hussain, Hammad Khan, Sabir Khan, Maria V.Boldrin Zanoni, Electrochemical preparation of Nb_2O_5 nanochannel photoelectrodes for enhanced photoelectrocatalytic performance in removal of RR120 dye, Chemosphere (2020), https://doi.org/10.1016/j.chemosphere.2020.127164.

[26] Osmando F. Lopes, Elaine C. Paris, Caue Ribeiro, Synthesis of Nb_2O_5 nanoparticles through the oxidant peroxide method applied to organic pollutant photodegradation: a mechanistic study, Appl. Catal. B Environ. (2014), https://doi.org/10.1016/j.apcatb.2013.08.031.

[27] Junqing Yan, Guangjun Wu, Naijia Guan, Landong Li, Nb_2O_5/TiO_2 heterojunctions: synthesis strategy and photocatalytic activity, Appl. Catal. B Environ. (2014), https://doi.org/10.1016/j.apcatb.2014.01.049.

[28] Sze-Mun Lama, Jin-Chung Sina, Ichikawa Satoshib, Ahmad Zuhairi Abdullaha, Abdul Rahman Mohamed, Enhanced sunlight photocatalytic performance over Nb_2O_5/ZnO nanorod composites and the mechanism study, Appl. Catal. A (2014), https://doi.org/10.1016/j.apcata.2013.12.001.

[29] L.M. Da Silva, L.A. De Faria, J.F.C. Boodts, Determination of the morphology factor of oxide layers, Electrochim. Acta (2001), https://doi.org/10.1016/S0013-4686(01)00738-1.

[30] A.J. Terezo, E.C. Pereira, Fractional factorial design applied to investigate properties of Ti/IrO_2-Nb_2O_5 electrodes, Electrochim. Acta. (2000), https://doi.org/10.1016/S0013-4686(00)00540-5.

[31] Ailton J. Terezo, Juan Bisquert, Ernesto C. Pereira, Germà Garcia-Belmonte, Separation of transport, charge storage and reaction processes of porous electrocatalytic IrO_2 and IrO_2/Nb_2O_5 electrodes, J. Electroanal. Chem. (2001), https://doi.org/10.1016/S0022-0728(01)00522-8.

[32] Fang Song, Lichen Bai, Aliki Moysiadou, Seunghwa Lee, Chao Hu, Liardet Laurent, Xile Hu, Transition Metal Oxides as Electrocatalysts for the Oxygen Evolution Reaction in Alkaline Solutions: an Application-Inspired Renaissance, J. Am. Chem. Soc. (2018), https://doi.org/10.1021/jacs.8b04546.

[33] Letícia Fernanda Gonçalves Larsson, Gideã Taques Tractz, Guilherme Arielo Rodrigues Maia, Guilherme José Turcatel Alves, Paulo Rogério Pinto Rodrigues, Maico Taras da Cunha and Everson do Prado Banczek, Comparative study of TiO2 and ZnO application in hybrid solar cells using copolymer P3OT/P3MT, (2019): https://doi.org/10.21577/0100-4042.20170344.

[34] Sumayya M. Abdulrahim, Zubair Ahmad, Muhammad Qasim, Sanghyun Mehmood, J. Bhadra. Paek, Noora J. Al-Thani, Mohammad Khaja Nazeeruddin, Abdelhak. Belaidi, Mahmood Amani, Effect of illumination and applied potential on the electrochemical impedance spectra in triple cation (FA/MA/Cs) 3D and 2D/3D perovskite solar cells, J. Electroanal. Chem. (2021), https://doi.org/10.1016/j.jelechem.2021.115800.

[35] Damien Voiry, Manish Chhowalla, Yury Gogotsi, Nicholas A. Kotov, Yan Li, Reginald M. Penner, Raymond E. Schaak, S. Paul, Best Practices for Reporting Electrocatalytic Performance of Nanomaterials, ACS Nano (2018), https://doi.org/10.1021/acsnano.8b07700.

[36] C.R. Zanata, P.S. Fernández, A.B. Santos, G.C.da Silva, G.A. Camara, C.A Martins, Estimating the Time-Dependent Performance of Nanocatalysts in Fuel Cells Based on a Cost-Normalization Approach, J. Braz. Chem. Soc. (2016), https://doi.org/10.5935/0103-5053.20160088.

[37] H. Ren, Y. Pan, C.C. Sorrell, H. Du, Assessment of electrocatalytic activity through the lens of three surface area normalization techniques, J. Mater. Chem. A (2020), https://doi.org/10.1039/c9ta13170a.

[38] C.C.L. McCrory, S. Jung, J.C. Peters, T.F. Jaramillo, Benchmarking Heterogeneous Electrocatalysts for the Oxygen Evolution Reaction, J. Am. Chem. Soc. (2013), https://doi.org/10.1021/ja407115p.

[39] Cancan Sun, Xiaodan Chen, Chenglong Ma, Limei Cao, Ji Yang, Pr-Si co-doped IrOx as promoted anode for refractory SDZ degradation, J. Electroanal. Chem. (2021), https://doi.org/10.1016/j.jelechem.2020.114954.

[40] S. Kang, J. Jang, S. Ahn, C.S. Lee, Novel design of hollow g-C_3N_4 nanofibers decorated with MoS_2 and S, N-doped graphene for ternary heterostructures, Dalton Trans. (2019), https://doi.org/10.1039/c8dt04656e.

[41] F. Xiong, D. Chen, C. Ma, L. Cao, J. Yang, Zr-Doped Ir as an Effective Anode for Refractory SMX Degradation, ACS Omega (2020), https://doi.org/10.1021/acsomega.9b03542.

[42] Panić, V., Dekanski, A., Mišković-Stanković, V.B., Milonjić, S., & Nikolić, B., On the deactivation mechanism of RuO2–TiO2/Ti anodes prepared by the sol–gel procedure, J. Elect. Chem.: 10.1016/j.jelechem.2005.01.026

[43] I.M.D. Gonzaga, A. Moratalla, K.I.B. Eguiluz, G.R. Salazar-Banda, P. Cañizares, M.A. Rodrigo, C. Saez, Outstanding performance of the microwave-made MMO-Ti/RuO_2-IrO_2 anode on the removal of antimicrobial activity of Penicillin G by photoelectrolysis, Chem. Eng. J. (2021), https://doi.org/10.1016/j.cej.2021.129999.

[44] D. Chen, Y. Cheng, N. Zhou, P. Chen, Y. Wang, K. Li, R. Ruan, Photocatalytic degradation of organic pollutants using TiO_2-based photocatalysts: a review, J. Clean. Prod. (2020), https://doi.org/10.1016/j.jclepro.2020.121725.

[45] G. Lu, Z. Lun, H. Liang, H. Wang, Z. Li, W. Ma, In situ fabrication of $BiVO_4$-$CeVO_4$ heterojunction for excellent visible light photocatalytic degradation of levofloxacin, J. Alloys Compd. (2018), https://doi.org/10.1016/j.jallcom.2018.09.064.

[46] L.A. Goulart, S.A. Alves, L.H. Mascaro, Photoelectrochemical degradation of bisphenol A using Cu doped WO_3 electrodes, J. Electroanal. Chem. (2019), https://doi.org/10.1016/j.jelechem.2019.03.027.

[47] C.H.M. Fernandes, B.F. Silva, J.M. Aquino, On the performance of distinct electrochemical and solar-based advanced oxidation processes to mineralize the insecticide imidacloprid, Chemosphere (2021) 130010, https://doi.org/10.1016/j.chemosphere.2021.130010.

[48] Xiuxiu Zeng, Xuelin Shi, Zhirong Sun, Degradation of atrazine by electroactivation of persulfate using FeCuO @ C modified composite cathode : synergistic activation mechanism, Chemosphere (2023) 138860, https://doi.org/10.1016/j.chemosphere.2023.138860.

[49] Panagiotis Lianos, Production of electricity and hydrogen by photocatalytic degradation of organic wastes in a photoelectrochemical cell The concept of the Photofuelcell: a review of a re-emerging research field, J. Hazard. Mater. 185 (2011) 575–590].

[50] Matheus S. Kronka, Guilherme V. Fortunato, Leticia Mira, Alexsandro J.dos Santos, Marcos R.V. Lanza, Using Au NPs anchored on ZrO_2/carbon black toward more efficient H_2O_2 electrogeneration in flow-by reactor for carbaryl removal in real wastewater, Chem. Eng. J. (2023), https://doi.org/10.1016/j.cej.2022.139598.

[51] Z. Frontistis, M. Antonopoulou, M. Yazirdagi, Z. Kilinc, I. Konstantinou, A. Katsaounis, & Mantzavinos, D, Boron-doped diamond electrooxidation of ethyl paraben: the effect of electrolyte on by-products distribution and mechanisms, J. Environ. Manage. (2017), https://doi.org/10.1016/j.jenvman.2016.06.044.

[52] M.N. Chong, B. Jin, C.W.K. Chow, & Saint, C, Recent developments in photocatalytic water treatment technology: a review, Water Res. (2010), https://doi.org/10.1016/j.watres.2010.02.039.

[53] N. Rioja, S. Zorita, F.J. Peñas, Effect of water matrix on photocatalytic degradation and general kinetic modeling, Appl. Catal. B Environ. (2016), https://doi.org/10.1016/j.apcatb.2015.06.038.

[54] C. Guillard, E. Puzenat, H. Lachheb, A. Houas, J.M. Herrmann, Why inorganic salts decrease theTiO_2 photocatalytic efficiency, Int. J. Photoenerg. (2005), https://doi.org/10.1155/s1110662x05000012.

[55] W.A. Adams, C.A. Impellitteri, The photocatalysis of N,N-diethyl-m-toluamide (DEET) using dispersions of Degussa P-25TiO_2 particles, J. Photochem. Photobiol. A Chem. (2009), https://doi.org/10.1016/j.jphotochem.2008.11.003.